

Online Supplementary Material to
**“Application of the reverberation waveform inversion for
the high-resolution sediment structure in the Pacific”**

HyeJeong Kim^{1,2,*}, Hitoshi Kawakatsu^{1,3}, Takeshi Akuhara¹, Nozomu Takeuchi^{1,*},
Takehi Isse¹, Hajime Shiobara¹, Hiroko Sugioka⁴, Hisashi Utada¹, YoungHee Kim⁵,
Sang-Mook Lee⁵

¹Earthquake Research Institute, University of Tokyo, 1-1-1 Yayoi, Bunkyo-ku, Tokyo 113-0032, Japan

²Department of Geology and Geophysics, The University of Utah, Salt Lake City, UT 84112, USA

³Institute of Earth Sciences, Academia Sinica, Taipei 11529, Taiwan

⁴Department of Planetology, Graduate School of Science, Kobe University, Kobe, Hyogo 657-8501, Japan

⁵School of Earth and Environmental Sciences, Seoul National University, Seoul 08826, Republic of Korea

Contents of this file:

Supplementary figures: Figures S1–S9

Supplementary tables: Tables S1–S5

References for the Supplementary Material

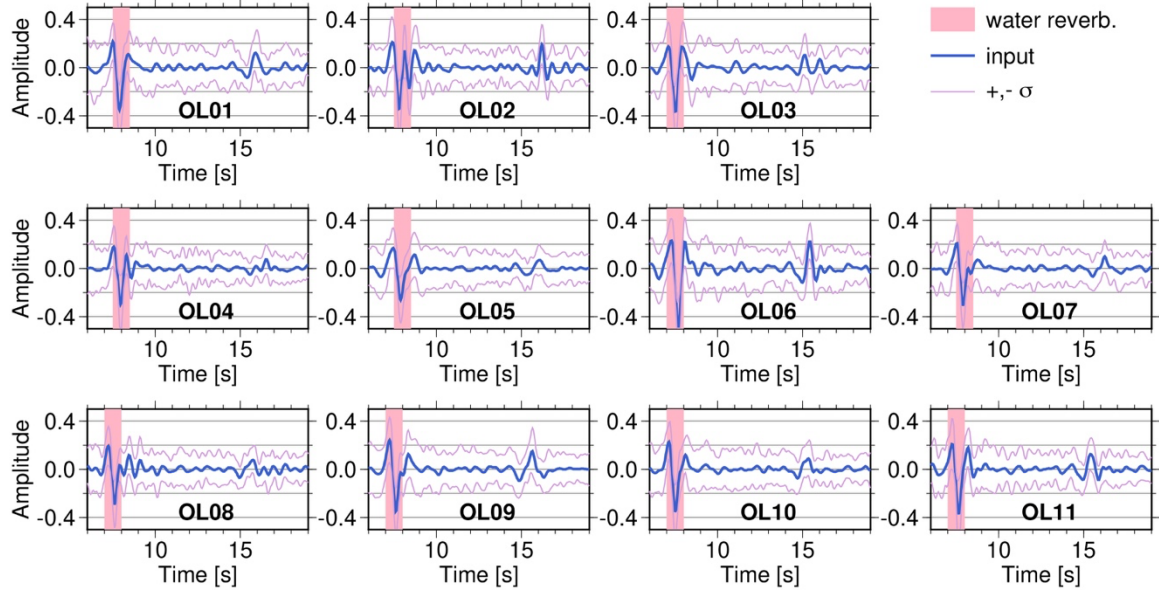


Figure S1. The stacked P-ACFs calculated using teleseismic P-waves (blue) at each station of the Oldest-1 array. The autocorrelation functions are calculated with the same parameters as Figure 2. The notations are the same as Figure 2 in the main text.

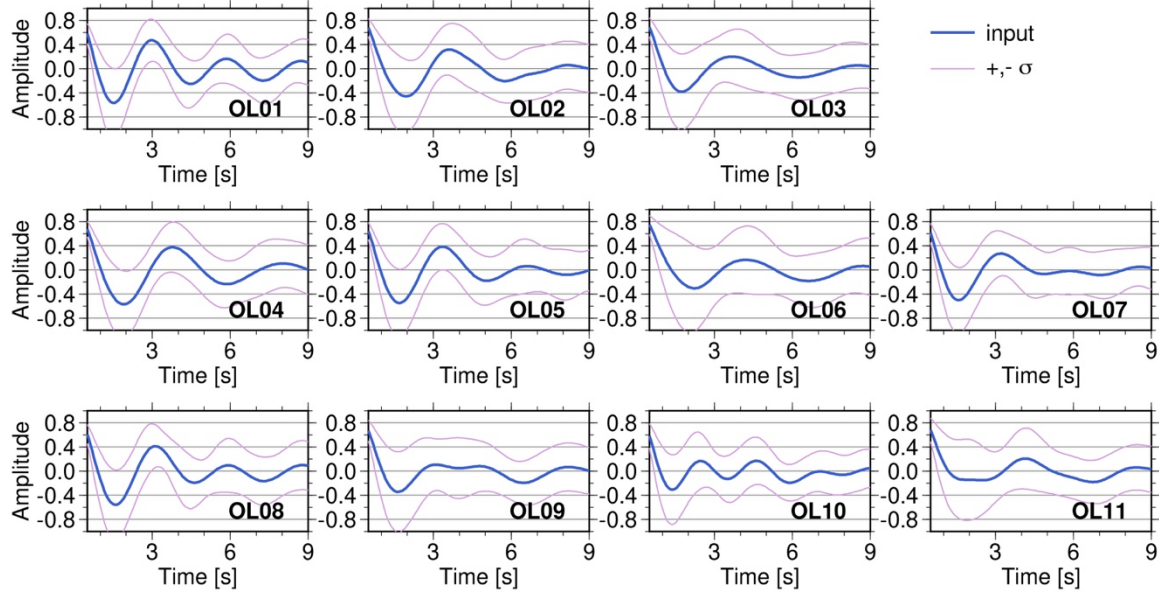


Figure S2. The stacked R-ACFs calculated using teleseismic S-waves (blue) at each station of the Oldest-1 array. Radial autocorrelation functions are calculated with the Gaussian low-pass parameter $a = 1.0$ and the whitening window width $W = 0.5$. The notations are the same as Figure 2 in the main text.

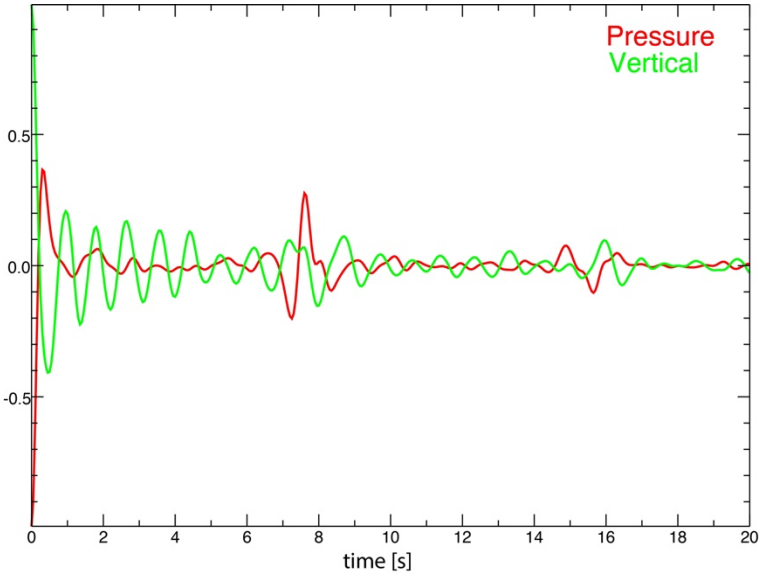


Figure S3. Autocorrelation functions of pressure (red) and vertical (green) components at station OL09. The first water reverberation at 7–8 sec is not clear on the vertical component, while it is evident on the pressure component.

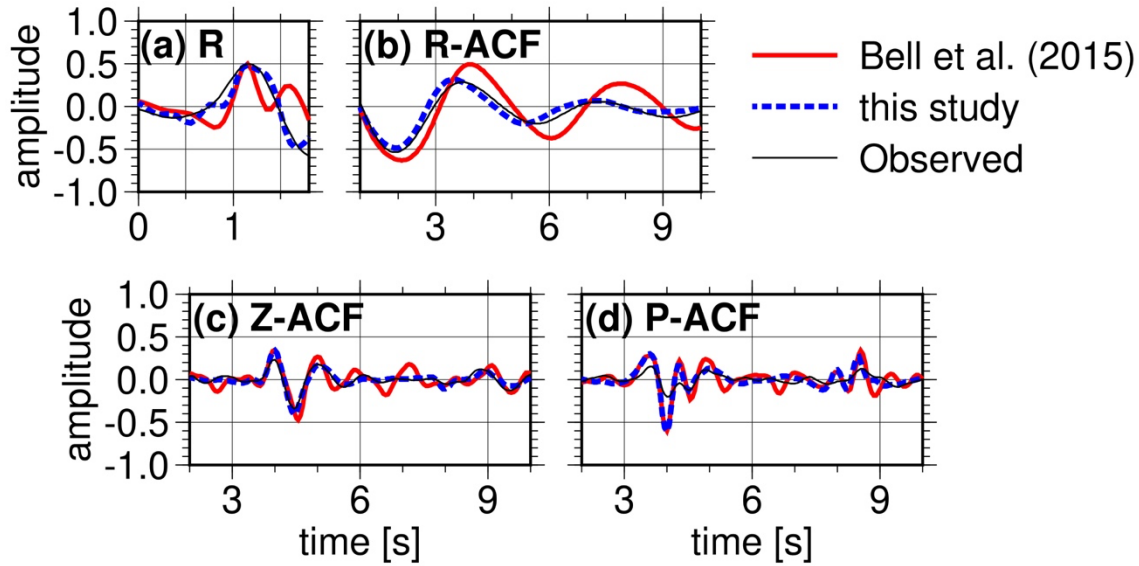


Figure S4. Synthetic waveforms at station J11D of the 7D array using sediment velocity models from Bell et al. (2015) and this study (“this study”) overlapped with the observed waveforms. Waveforms of (a) radial stack (R-stack), (b) radial autocorrelation function (R-ACF), (c) vertical autocorrelation function (Z-ACF), and (d) pressure autocorrelation function (P-ACF). (a,c–d) are calculated using incident P-wave with a ray parameter of 6.5×10^{-5} s/m. (b) is calculated with incident S-wave with a ray parameter of 1.2×10^{-4} s/m. (a) is band-pass filtered with 0.1–1.0 Hz, (b) is low-pass filtered with Gaussian low-pass filter parameter $a = 2.5$ and calculated with smoothing width $W = 0.5$, and (c,d) are

low-pass filtered with Gaussian low-pass filter parameter $a = 5.0$ and calculated with smoothing width $W = 0.8$.

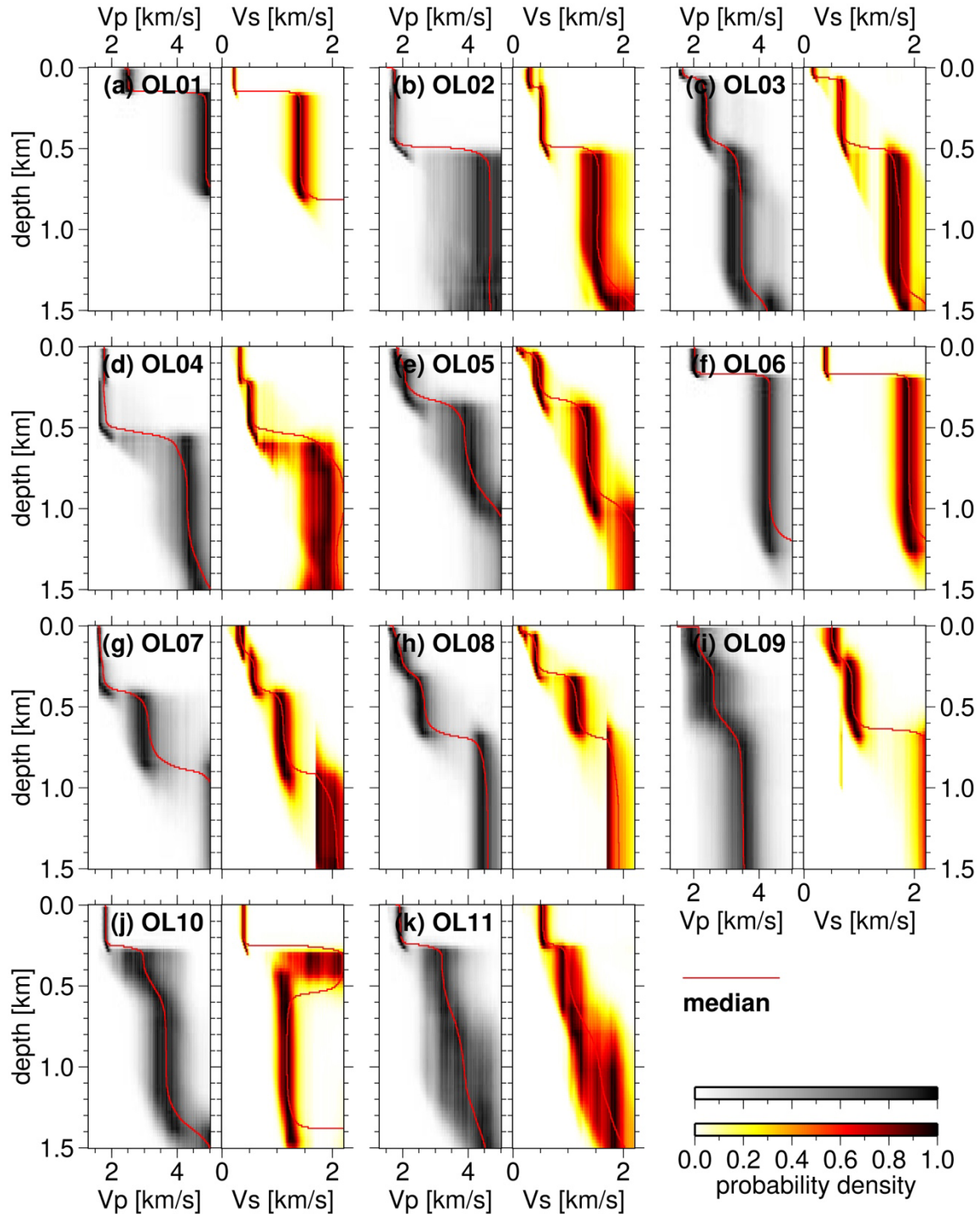


Figure S5. P-wave velocity (V_p) and S-wave velocity (V_s) by depth profiles at each station of the Oldest-1 array. Solid lines indicate median probability velocity profiles and

shaded background show the probability density function by depth. The station map is in Figure S6.

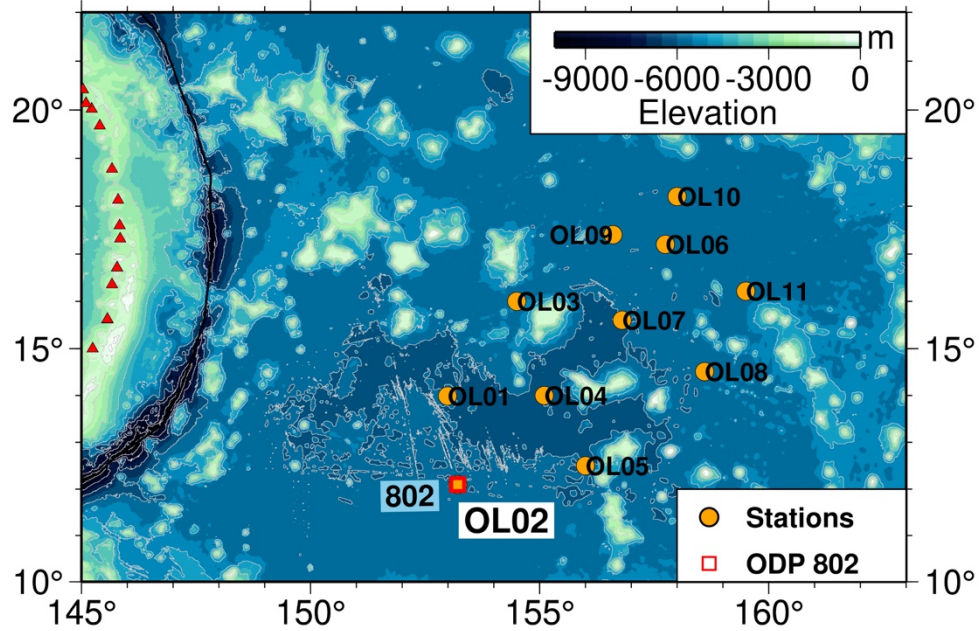


Figure S6. Map showing Oldest-1 array stations. Location of the nearest drilling site is marked with a red square and the stations are marked with orange circles.

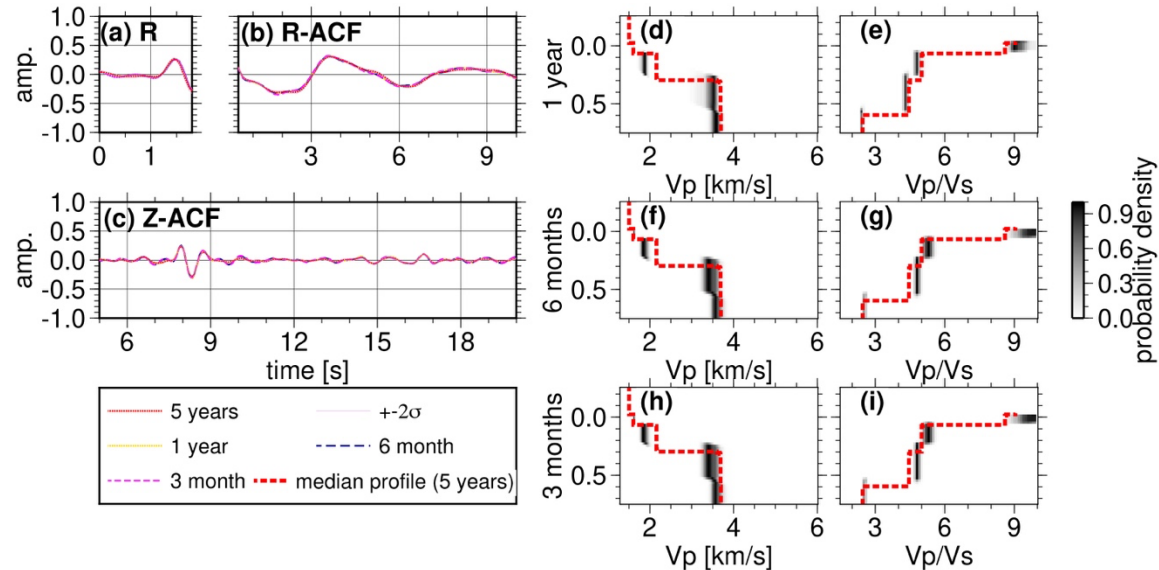


Figure S7. Results of S6N09 inversion using shorter time spans, 1-year (2019.01–12), 6-months (2019.07–12), and 3-months (2019.07–09). The result of 5-year-long data is identical to Figure 10 in the main text. Input (a) R-stack, (b) R-ACF, and (c) Z-ACF waveforms of different time spans. (d, f, h) P-wave velocity probability density functions from inversions of 1-year, 6-month, and 3-month, overlain by the V_p median probability profile from the 5-year inversion. (e, g, i) P-wave velocity probability density functions from inversions of 1-

year, 6-month, and 3-month, overlain by the V_P/V_S median probability profile from the 5-year inversion.

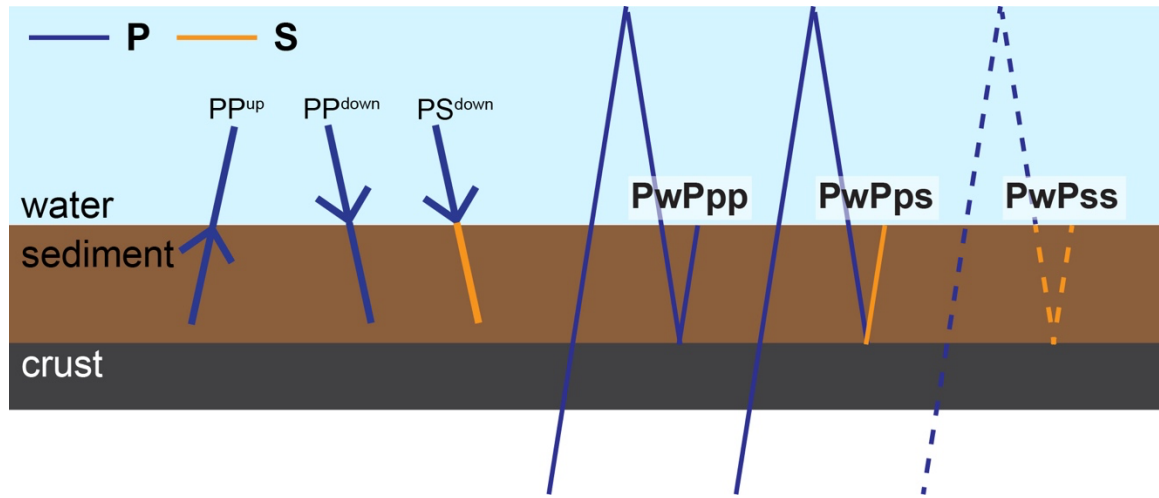


Figure S8. A schematic cartoon showing the rays considered in Figure 11b. The direction of the arrow points to the direction of the propagation; dark blue lines and light orange lines mark the propagating P wave and S wave, respectively. The top light blue layer is the water layer, the dark brown layer in the middle is the sediment layer, and the dark gray layer in the bottom is the crust layer.

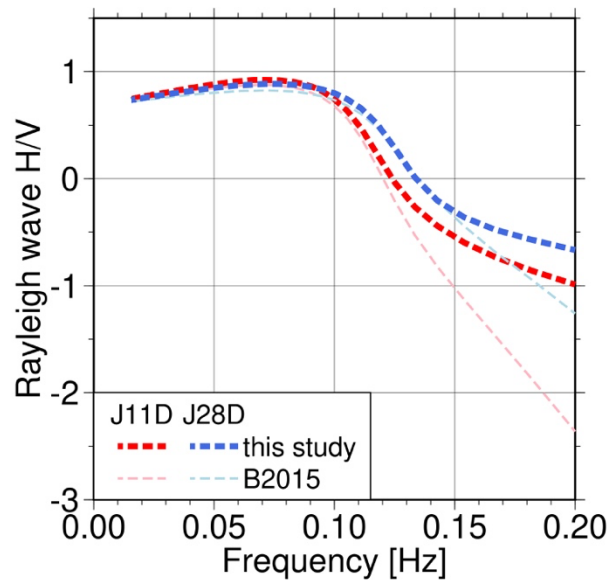


Figure S9. Predicted Rayleigh-wave ellipticity (i.e., radial to vertical ratio) of the fundamental mode Rayleigh-wave using the sediment models of Bell et al. (2015) and this study. The crust and upper mantle layers in Bell et al. (2015) are added below the sediment model of this study for the computation. The difference between two predictions in frequencies above 0.10 Hz indicate that sediment models which had

general agreement in Rayleigh-wave admittance can be resolved using the Rayleigh-wave ellipticity.

array name	operating period	# of stations	available models	Sensor Types	Country of origin
Oldest-1	2018-10-31–2019-11-04	11	ODP 802 (Lancelot et al., 1990)	Guralp CMG-3T	Japan
OJP	2014-11-17–2016-09-30	16	Tonegawa et al. (2019)		Japan
PLATE (Z6)	2009-10-22–2010-10-31	3	ODP 878 (Premoli Silva et al., 1993)	Nanometrics Trillium 240 s and 40 s	US
PLUME (YS)	2006-04-12–2007-06-06	2	Doran & Laske (2019), ODP 843 (Dziewonski et al., 1992) DSDP 67 (Winterer et al., 1971)	Guralp CMG-3T	US
Cascadia Initiative (7D)	2014-07-11–2015-09-01	2	Ruan et al. (2014), Bell et al. (2015)	Nanometrics Trillium Compact	US
S-net	2017-04-13–2022-05-22	1	Fujie et al. (2013), Nakamura et al. (2014)	OYO Geospace OMNI-2400	Japan (online cable network)

Table S1. List of ocean bottom seismometer arrays used in this study. Arrays obtained from the IRIS MetaData Aggregator have network codes in parentheses. Studies with available seafloor sediment models around the stations and the country of origin of the instrumentation is specified on the right side of the table.

Array or station	Band pass filter used for R-stack (Hz)	Gaussian low-pass filter parameter used for R-ACF	High-pass filter used for R-ACF (Hz)
Oldest-1	0.1–1.0	$a = 1.0$	N/A
OJP	0.5–2.0	$a = 1.0$	N/A
Z6	0.5–2.0	$a = 2.5$	0.05
YS (PL37)	0.5–2.0	$a = 2.5$	0.1
YS (PL46)	0.5–2.0	$a = 2.5$	0.05
7D	0.5–2.0	$a = 1.0$	0.05
S-net	0.5–2.0	$a = 2.5$	N/A

Table S2. List of frequency contents used in the analysis of ocean bottom seismometers.

	R-stack	R-ACF	Z-ACF
2017.04–2022.05	80	210	137
2019.01–12	26	48	31
2019.07–12	20	26	19
2019.07–09	18	21	16

Table S3. Numbers of teleseismic event waveforms stacked for the shorter operation period analysis with station S6N09 (Figure S7).

layer	Density [kg/m ³]	Vp [m/s]	Vs [m/s]
sediment	2000	2000	X
crust	2600	5800	3200

Table S4. Physical parameters of the layers used for calculating the expected amplification due to S transmission coefficients. The S-wave velocity of the sediment varies following the x-axis of Figure 11a. The slowness used for the calculation is 6.0×10^{-5} s/m.

layer	Density [kg/m ³]	Vp [m/s]	Vs [m/s]
water	1030	1500	0
sediment	Brocher (2005)		
crust	3300	6800	3930
mantle	3300	8200	4620

Table S5. The model used for calculating transmission coefficients in Figure 11b. The slowness used for the coefficient calculation is 6.5×10^{-5} s/m.

layer	Thickness [km]	Density [kg/m ³]	Vp [m/s]	Vs [m/s]
Upper Crust	2	2450	5000	2630
Lower Crust	5	3050	6800	3890
Uppermost mantle	20	4326	7913	3270

Table S6. Crust and mantle layers added to the sediment model to compute Rayleigh wave predictions in Figures 12 and S8. For models from this study, we replaced the Upper Crust density and velocities using half-space crust layer density and velocities from the inversion. These layered are assumed during the Rayleigh wave admittance inversion in Ruan et al. (2014) and Bell et al. (2015).

References From the Supplementary Material

- Bell, S. W., Ruan, Y., & Forsyth, D. W., 2015. Shear Velocity Structure of Abyssal Plain Sediments in Cascadia. *Seismological Research Letters*, 86 (5), 1247–1252. doi: <https://doi.org/10.1785/0220150101>.
- Brocher, T. M., 2005. Empirical Relations between Elastic Wavespeeds and Density in the Earth's Crust. *Bulletin of the Seismological Society of America*, 95 (6): 2081–2092. doi: <https://doi.org/10.1785/0120050077>
- Doran, A. K., & Laske, G., 2019. Seismic structure of marine sediments and upper oceanic crust surrounding Hawaii. *Journal of Geophysical Research: Solid Earth*, 124, 2038–2056. <https://doi.org/10.1029/2018JB016548>
- Dziewonski, A. M., Wilkens, R. H., Firth, J. V., Baker, D. J. J., Briden, J. C., Carson, B., ... Winkler, W., 1992. Site 843. Proceedings of the Ocean Drilling Program, Part A: Initial Reports, Vol. 136, p.65-99. doi:10.2973/odp.proc.ir.136.105.1992
- Fujie, G., Kodaira, S., Yamashita, M., Sato, T., Takahashi, T., & Takahashi, N., 2013. Systematic changes in the incoming plate structure at the Kuril trench. *Geophysical Research Letters*, 40, 88–93, 10.1029/2012GL054340.
- Lancelot, Y. P., Larson, R., Fisher, A., Abrams, L., Behl, R., Busch, W. H., ... Dearmont, L. H. (1990). Site 802. Proceedings of the Ocean Drilling Program, Part A: Initial Reports, Vol. 129, p.171-243. doi:10.2973/odp.proc.ir.129.104.1990
- Nakamura, Y., Kodaira, S., Cook, B.J. Jeppson, T., Kasaya, T. et al., 2014. Seismic imaging and velocity structure around the JFAST drill site in the Japan Trench: low Vp, high Vp/Vs in the transparent frontal prism. *Earth, Planets and Space*, 66, 121. <https://doi.org/10.1186/1880-5981-66-121>
- Premoli Silva, I., Haggerty, J. A., Rack, F. R., Arnaud-Vanneau, A., Bergersen, D. D., Bogdanov, Y., ... Maddox, E. M., 1993. Site 878. Proceedings of the Ocean Drilling Program, Part A: Initial Reports, Vol. 144, p.331-412. doi:10.2973/odp.proc.ir.144.111.1993
- Ruan, Y., Forsyth, D. W., & Bell, S. W., 2014. Marine sediment shear velocity structure from the ratio of displacement to pressure of Rayleigh waves at seafloor. *Journal of Geophysical Research: Solid Earth*, 119(8), 6357-6371. doi: 10.1002/2014JB011162
- Tonegawa, T., Miura, S., Ishikawa, A., Sano, T., Suetsugu, D., Isse, T., & Kobayashi, T., 2019. Characterization of crustal and uppermost mantle seismic discontinuities in the Ontong Java Plateau. *Journal of Geophysical Research: Solid Earth*, 124(7), 7155-7170. <https://doi.org/10.1029/2018JB016970>
- Winterer, E. L., Riedel, W. R., Gealy, E. L., Heath, G. R., Kroenke, L. W., Martini, E., ... Moberly, R., Jr., 1971. Site 67. Initial Reports of the Deep Sea Drilling Project, p.821-841. doi:10.2973/dsdp.proc.7.109.1971